


Large tunable exchange fields due to purely paramagnetically limited domain wall superconductivityPushpak Banerjee ¹, Pramod K. Sharma,¹ Sonam Bhakat,¹ Biswajit Dutta,¹ and Avradeep Pal^{1,2,*}¹*Department of Metallurgical Engineering and Materials Science, Indian Institute of Technology, Bombay, Mumbai, Maharashtra 400076, India*²*Centre of Excellence in Quantum Information, Computation, Science and Technology, Indian Institute of Technology, Bombay, Mumbai, Maharashtra 400076, India*

(Received 8 November 2022; revised 29 July 2023; accepted 28 August 2023; published 4 October 2023)

The ability to apply and tune large magnetic fields locally is a crucial requirement for several devices, most notably for the detection and generation of Majorana fermions. Such a functionality can be achieved in superconductor (S)/ferromagnet (F) bilayers, where superconductivity is strengthened on top of domain walls due to local lowering of the proximity-induced effective exchange fields. By using niobium and ferromagnetic insulating (GdN) bilayers, and through detailed magnetotransport measurements, we demonstrate the phenomena of switching in and out of the domain wall superconducting phase in S/F bilayers by purely paramagnetic tuning of induced exchange fields. In the thinnest of niobium layers, we estimate that this tunability can be as high as 1.3 T with the application of in-plane external fields of a few milliteslas.

DOI: [10.1103/PhysRevB.108.L140502](https://doi.org/10.1103/PhysRevB.108.L140502)

Thin-film superconductor (S)/ferromagnet (F) systems have been studied extensively due to the possibility of detection of novel interfacial effects and prospective dissipationless device functionalities [1]. Notable among these are $0-\pi$ transitions [2–4], resulting in an oscillatory order parameter, and the generation of long-range odd-frequency triplet correlations [5–8]. However, one of the longstanding theoretical predictions that has eluded experimental observation is that of a purely magnetic domain state mediated and purely paramagnetically limited switching of the superconducting state to the normal state and vice versa in S/F bilayers [9,10].

In S/F bilayers, Cooper pairs interact with the ferromagnet either through a proximity-induced exchange field, causing paramagnetic pair breaking [9,10] or with stray magnetic fields emanating from the ferromagnet, resulting in orbital pair breaking [11]. As opposed to orbital pair breaking [12,13], paramagnetic pair breaking is especially useful for the tuning of induced exchange fields, with the superconductor remaining homogeneous, but with a reduced energy gap. When the underlying ferromagnet transitions into a multidomain state, it results in areas over domain walls with reduced pair-breaking exchange fields, thus resulting in a reduced average effective exchange field in the superconductor layer. The difference in average exchange fields in the saturated and multidomain state of the ferromagnet is tantamount to exchange-field tunability in the superconductor layer. This can result in a superconducting phase in the multidomain state and a normal state in the saturated state of the ferromagnet. This translates into a measurable difference in the critical temperature (T_c) in the saturated and coercive states of the ferromagnet. Such T_c differences can be analyzed with theoretically predicted normal to superconducting (N-S)

phase diagrams of high field superconductivity and paramagnetically limited domain wall superconductivity (DWS) to estimate the tunability of the exchange field in the system. Thus far, experiments investigating paramagnetic pair breaking in S/F bilayers have been shown to cause minimal N-S transitions [14–16], with very low differences in T_c (30 mK or less), and hence magnitudes of exchange-field tunability have not been derived. In this Letter, we fill this experimental gap using Nb/GdN bilayers and demonstrating a purely proximity-induced, exchange-field, modification-driven N-S transition of thin-film niobium by applying small fields (a few milliteslas) that alter the domain state of a thin-film soft ferromagnetic insulator (FI): GdN.

As opposed to a metallic ferromagnet, in S/FI systems, the situation is slightly different. When measured in current in-plane geometry, with thin superconductor layers, electrons of the Cooper pair undergo reflections at the S/FI interface [17]. This leads to an exchange interaction that manifests as an effective exchange field in the thin superconductor layer. However, a FI layer prevents diffusion of Cooper pairs into itself, and therefore this constitutes a purely interfacial, proximity-induced exchange-field effect [17–19]. The superconducting coherence length (ξ_T) at a temperature (T) close to the transition temperature (T_c) abides by the Ginzburg-Landau (GL) relation,

$$\xi_T = \frac{\xi_{T=0}}{\sqrt{\frac{\Delta T}{T_c}}} \quad (1)$$

where $\Delta T = |T_c - T|$. When the Cooper pair interacts with FI moments in a single domain, it experiences a uniform exchange field that contributes to the paramagnetic pair-breaking effect and leads to a quasiparticle spin split superconducting state [20,21]. The Cooper pairs can also sample the moments of two adjacent domains if ξ_T lies in

*avradeep@iitb.ac.in

a range between the domain wall width (d_w) and the modal lowest dimension of the domains. In this scenario, the effective exchange field would reduce, resulting in reduced paramagnetic pair breaking, which, as described earlier, is measurable through an enhanced T_c of the system [9,10].

This phenomena of DWS, although in spirit is very similar, it is microscopically distinct from the spin switch effect in F/S/F trilayers [22], where switching the direction of the magnetic moment of the soft ferromagnet layer in comparison to a harder ferromagnet layer causes a T_c enhancement due to overall relative parallel and antiparallel arrangements of the two ferromagnets, which are approximated to be macrospins, without their finer domain texture. Moreover, as opposed to F/I/S bilayers, where the field-tunable superconductor layer can be interfaced with other device components (for example, a nanowire in the case of Majorana devices), F/S/F trilayers may not be useful for applications seeking local field tunability.

In addition to filling the experimental gap of precisely measuring exchange-field tunability, we also test the predictions of the theory of paramagnetically limited DWS by controllably tuning the following intrinsic physical parameters: ξ_T , $\xi_{T=0}$, and the domain wall area fraction. This can be done by varying the corresponding experimental parameters—temperature (T) for changing ξ_T and superconducting niobium film thickness [23], which affects $\xi_{T=0}$ in the dirty limit—and externally applying a magnetic field (H) that affects the domain state of the ferromagnet.

Multilayers of the form AlN (10 nm)/Nb (varying thickness)/GdN (3 nm)/AlN (15 nm) were grown on n -doped Si/SiO₂ (285-nm) substrates via magnetron sputtering inside a custom-made multitarget UHV chamber with a base pressure on the order 10^{-9} mbar. GdN and AlN layers were deposited using reactive dc sputtering of gadolinium and aluminum in an 8% and 44%, respectively, N₂-in-argon atmosphere at 1.5 Pa. Niobium thickness was varied by keeping samples in a rotating table and rotating them under a masking plate under the niobium targets using a computer-controlled stepper motor. Magnetization measurements as a function of in-plane magnetic fields were performed on AlN/GdN(3nm)/AlN samples using a vibrating sample magnetometer (VSM), the MPMS3 SQUID VSM from quantum design. For the magnetotransport measurements, the stacks were wire-bonded in four-point geometry, glued to custom-made printed circuit boards devoid of any magnetic material, and affixed to a probe that was inserted into a variable temperature inset of an Oxford Teslatron pulse tube cryostat, and uniaxial magnetic fields were applied using the built-in superconducting solenoid of the Teslatron system. The QCODES platform was adopted for data acquisition.

In Fig. 1(a), we measure resistance (R) with increasing temperatures at several values of externally applied magnetic fields, from positive to negative saturation and vice versa. The sharp horn-like features are suggestive of how the T_c enhancement is correlated to the coercive field of the FI. The T_c enhancement can also be visualized from isolated R - T plots (extracted vertical linecuts) as shown in Fig. 1(b). The R - H plot in Fig. 1(c) represents a horizontal linecut of the color map at 4.2 K, and shows the transition to the DWS phase, which coincides with the magnetization switching field values obtained from the VSM measurements of a 3-nm GdN film

without the top niobium layer. Figure 1(d) shows an identical measurement of a sample in which the interface between GdN and niobium is broken by 3 nm of insulating AlN and which is grown in the same growth run, with the same plasma for GdN and niobium. However, the T_c of the system is far greater than without AlN in between, and the horn-like features are missing. This demonstrates the purely interfacial nature of the effect, and the minimal role of orbital pair breaking caused by stray fields.

Next we discuss the origin of the horn-like features in greater detail. The following five considerations are central to the understanding of these features:

(1) Copper pairs are most stable when two opposite spins constituting it lie in a neighborhood of like spins [10] [for example, the starred event in Fig. 1(e), which shows a Cooper pair just large enough to be lying on the boundary of an in-plane domain wall]. This is the condition when the exchange field it experiences is the lowest.

(2) As temperature is increased, Cooper pair size increases continuously, which may lead to the following conditions: initially, $\xi_T < d_w$, followed by $\xi_T \sim d_w$ [starred event of Fig. 1(e)], and finally $\xi_T \gg d_w$.

(3) As the field is lowered from saturation, the number of domains increases, and this increases the frequency of the starred event shown in Fig. 1(e).

(4) Hence, Cooper pair stability (and therefore T_c) will be highest when $\xi_T \sim d_w$, and the external applied field equals the coercive field. Hence the sharp increase of T_c at coercive fields on either side.

(5) The effect fades out if $\xi_T \gg d_w$. In this condition, after increasing temperatures, a Cooper pair has become so large that it is no longer lying across the boundary of one single domain wall with opposite spin orientation on either sides. Hence, T_c does not increase indefinitely.

The situation, specifically at $\xi_T \sim d_w$, for various fields is represented by Fig. 1(e). At saturation fields, the Cooper pairs face a uniform exchange field, and this becomes spatially nonuniform at the coercive fields. The nonuniformity causes a net lowering of the exchange field and is ultimately tantamount to exchange-field tunability.

In Fig. 2, we plot the dependence of various properties as a function of niobium thickness. T_c suppression of niobium due to the proximity effect of GdN is clearly visible in Fig. 2(a). Above 20 nm, no discernible horn-like features were observed, and below 7 nm, the bilayers showed no superconducting transitions until 0.25 K. Please refer to Supplemental Material Fig. S1 [24] for color maps of samples at these two extremes. The two noticeable aspects of thickness dependence present in Fig. 2(b) are (i) the rapid decrease of the T_c enhancement effect with increasing thickness [evident through both $\Delta T/T_c = (T_{\text{Sat}} - T_{\text{Coer}})/T_{\text{Sat}}$ and $\Delta T = (T_{\text{Coer}} - T_{\text{Sat}})$ data, where T_{Coer} and T_{Sat} are the transition temperatures at the coercive field and saturation field, respectively] and (ii) the reduced T_c of Nb/GdN films compared to identical film-layer thickness, but with a thin 3 nm of insulating AlN in between GdN and niobium [Fig. 2(b), inset]. With reference to the latter observation, we also note that the magnitude of the T_c decrease is highest for the thinnest niobium films. We attribute this to the lowering of the average proximity-induced exchange fields with increasing niobium

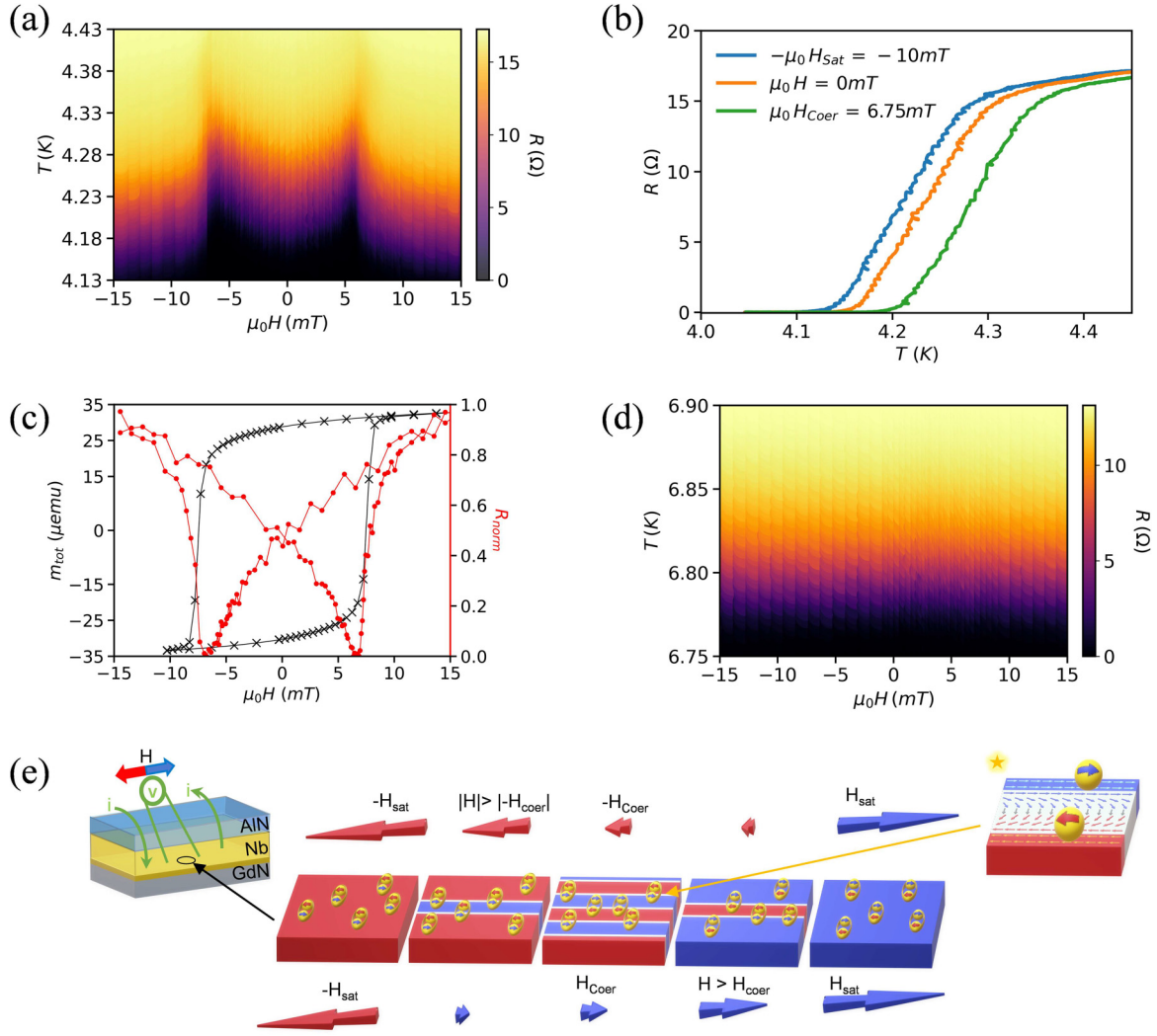


FIG. 1. (a) Resistance $R(\Omega)$ of Nb (8 nm)/GdN (3 nm) versus the applied field $\mu_0 H$ (mT) and temperature T (K) represented for the field sequence $0 \rightarrow H_{\text{Coer}} \rightarrow +H_{\text{Sat}}$ and $0 \rightarrow -H_{\text{Coer}} \rightarrow -H_{\text{Sat}}$. (b) R - T plots for H_{Sat} , zero field, and H_{Coer} . (c) Normalized resistance R_{norm} versus $\mu_0 H$ (mT) (red circles) and magnetic moment m_{tot} (μemu) versus $\mu_0 H$ (mT) (black cross) for a GdN (3-nm) film at 4.2 K. (d) R - T versus H color map with a sequence of -15 mT to 15 mT for a Nb (8-nm)/AlN (3-nm)/GdN (3-nm) stack. (e) Illustration of DWS phenomena depicting the interaction of Cooper pairs with a micromagnetic structure at the interface of niobium and GdN. The yellow star denotes a particular event when $\xi_T \sim d_w$.

thickness [17]. The former observation is due to the reduction of the mean free path ℓ , as shown in Fig. 2(d), of niobium with reducing niobium film thickness, which in turn reduces the zero-temperature dirty limit coherence length $\xi_{T=0}$ since $\xi_{T=0} \sim 0.855\sqrt{\xi_0\ell}$ where ξ_0 is the bulk coherence length. The mean free path corresponding to niobium films of the reported thickness was estimated from residual resistivity measurements [shown in Fig. 2(d), inset] (ρ_{10K}) [23,25]. We found at least two accounts of such a thickness dependence of the niobium mean free path in the literature [23,26]. The perpendicular to the plane critical-field measurements [Fig. 2(c)] also yielded a set of coherence length values ($\xi_{T=0}$) using the following relations:

$$H_{C2\perp}(T=0) = \frac{\phi_0}{2\pi\xi_{T=0}^2} \quad (2)$$

and

$$H_{C2\perp}(T) = H_{C2\perp}(T=0) \frac{1 - (T/T_c)^2}{1 + (T/T_c)^2}. \quad (3)$$

Here, T_c is the transition temperature of the bilayer samples at zero field [Fig. 2(a)], and T (~ 1.6 K) is the temperature at which the RH_{\perp} measurements [Fig. 2(c), inset] were taken. While the values of ξ_T derived from two different kinds of measurement are not identical, the trend of an overall, largely monotonic, increase of ξ_T with niobium thickness is seen in both kinds of measurement. Moreover, we point out that the discussion regarding what constitutes $H_{C2\perp}$ in a system with an intrinsic exchange field might be a little more nuanced, and is beyond the purview of this reported work. We hence take greater cognizance of the values of ξ_T obtained from residual resistivity and mean free path measurements.

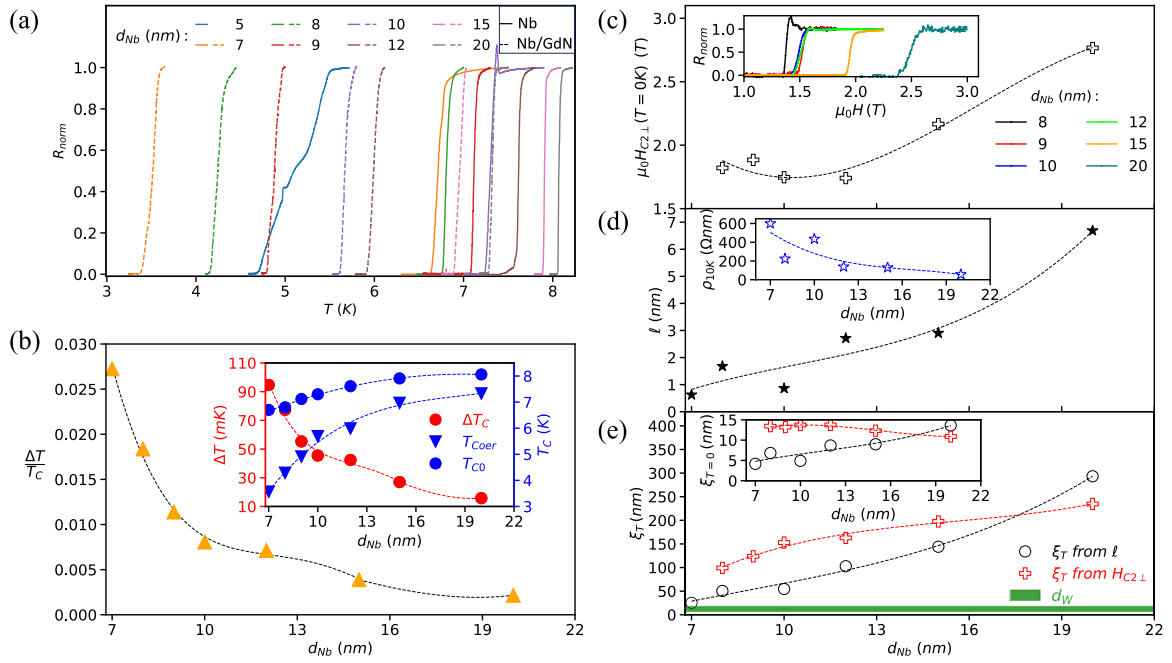


FIG. 2. (a) R - T plots displayed as solid lines for bare niobium films and dashed lines for Nb/GdN bilayers. (b) $\frac{\Delta T}{T_c}$ (orange triangles) versus d_{Nb} . Inset: Red circles show the dependence of ΔT on d_{Nb} , blue circles represent T_{Co} of Nb/AlN/GdN, and blue triangles represent T_{Coer} of Nb/GdN stacks. (c) Projected $H_{\text{C}2\perp}$ at 0 K is marked with unfilled plus signs. Inset: The R - H_{\perp} plots at 1.6 K used for estimating $H_{\text{C}2\perp}$ are provided. (d) Black stars represent the calculated mean free path (ℓ) at 10 K from the residual resistivity measurements, which are denoted by blue unfilled stars (inset). (e) Black unfilled circles represent ξ_T calculated from ℓ and $\frac{\Delta T}{T_c}$. The unfilled red plus signs represent ξ_T derived from $H_{\text{C}2\perp}$ measurements. The green band represents the range of possible domain wall widths (d_w). Inset: The corresponding $\xi_{T=0}$ values.

It is expected that the largest T_c enhancements should occur when the GL coherence length [ξ_T from Eq. (1)] close to T_{Coer} is comparable to domain wall width $d_w = \pi \sqrt{\frac{A}{K_u}}$, where A is exchange stiffness coefficient and K_u is the uniaxial magnetocrystalline anisotropy of the FI layer. We estimate d_w from calculations of A and K_u available in the literature [27,28], and present it as a spread of values in Fig. 2(e). We observe that the limit $\xi_T \cong d_w$ is satisfied for the lowest thicknesses ($T = 3.57$ K), and gradually settles to $\xi_T \gg d_w$ ($T = 7.33$ K). This observation tallies with decreasing ΔT with increasing niobium thickness, as the effect of domain wall-induced Cooper pair stability is reduced for larger Cooper pairs in thicker niobium. Although increasing superconducting thickness always corresponds to decreasing proximity effects, our experiment suggests that for a FI layer with a larger d_w , the range of niobium thicknesses for which the effect can be observed may be higher than 20 nm.

We next probe the influence of the texture of the proximity-induced exchange field on the nature of the S-N phase transition. This is best portrayed through the theory of localized, nonuniform DWS put forth by Houzet-Buzdin (H-B) [10], as compared to the uniform high-field superconductivity treatments by Maki-Fulde (M-F) [29–31].

For this analysis, we trace out the phase diagram for domain wall-induced nonuniform superconductivity [10], and superimpose our $T/T_{\text{c0}} = \frac{T_{\text{Nb/GdN}}}{T_{\text{AlN/GdN}}}$ data on it in Fig. 3.

We assume that $T = T_{\text{Sat}}$ (blue stars in Fig. 3) corresponds to the M-F curve, whereas $T = T_{\text{Coer}}$ (green unfilled stars) corresponds to the H-B curve. The net exchange field is reduced

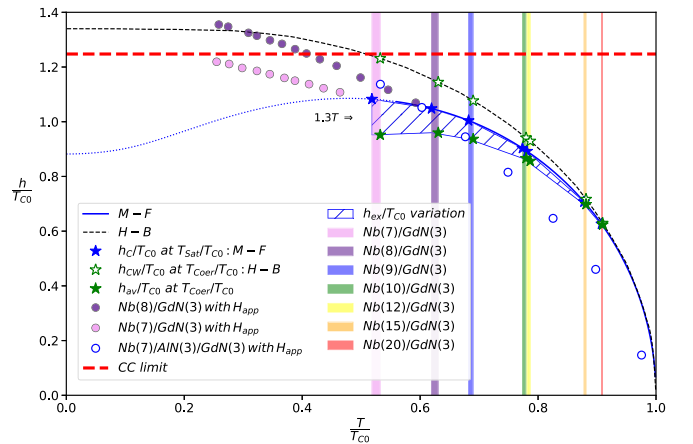


FIG. 3. The black dashed curve represents the H-B boundary for DWS. The blue curve is the M-F phase boundary for uniform superconductivity. The colored bands (violet, purple, blue, green, yellow, orange, and red, starting from the left) represent $\frac{T_{\text{Coer}} - T_{\text{Sat}}}{T_{\text{c0}}}$ for Nb/GdN films (niobium, 7 to 20 nm). Blue filled stars at $(\frac{h_c}{T_{\text{c0}}}, \frac{T_{\text{Coer}}}{T_{\text{c0}}})$ of Nb/GdN correspond to the critical exchange field ($\frac{h_c}{T_{\text{c0}}}$) on the M-F curve. The green unfilled stars represent $\frac{T_{\text{Coer}}}{T_{\text{c0}}}$, which is used to estimate $\frac{h_{\text{Coer}}}{T_{\text{c0}}}$ on the H-B curve. The green filled stars are the derived average exchange fields ($\frac{h_{\text{av}}}{T_{\text{c0}}}$) at $\frac{T_{\text{Coer}}}{T_{\text{c0}}}$. The hatched region denotes variation in the exchange field ($\frac{h_{\text{ex}}}{T_{\text{c0}}}$). The filled violet and purple circles, and the unfilled blue circles represent $\frac{h}{T_{\text{c0}}}$ from in-plane critical fields for Nb (7 nm)/GdN (3 nm), Nb (8 nm)/GdN (3 nm), and Nb (7 nm)/AlN (3 nm)/GdN (3 nm), respectively. The red dashed line represents the normalized paramagnetic limit of around $1.25 T_{\text{c0}}$.

due to the presence of domain walls, whereas the values in the H-B curve indicate an increase in effective exchange fields. This contradiction can be overcome from consideration of the parameters that go into the model underpinning the H-B curve and their implications. In the M-F theory, h_C is the magnitude of the exchange field vector. In the absence of domain walls, this vector is uniform throughout. Hence, the magnitude of an induced exchange field at $T=T_{\text{Sat}}$, can be extracted from the M-F phase boundary. We find that although h_C for all samples (blue stars in Fig. 3) is of the order of several Tesla, it is always less than the internal molecular field for GdN ($T_{\text{Curie}} \approx 35$ K), which we estimate as 17.3 T from the Curie-Weiss theory.

In the presence of domain walls, over several regions, the net exchange field on a Cooper pair reduces [starred event in Fig. 1(e)]. Nevertheless, the H-B theory proposes a net vector of magnitude h_{cw} that can account for the decreased area average exchange field (h_{av}). The previous implies the following set of relations:

$$h_{av} < h_C. \quad (4)$$

From observation of the fact that H-B curve is always higher than M-F curve, we posit

$$h_{cw} = f h_C, \text{ where } f > 1. \quad (5)$$

Therefore from Eqs. (4) and (5), we logically deduce that

$$h_{av} = h_C / f. \quad (6)$$

Hence, the tunability of exchange field h_{ex} is

$$h_{ex} = h_C - h_{av} = \left(1 - \frac{1}{f}\right) h_C. \quad (7)$$

This variation of h_{ex} of the effective proximity-induced exchange field due to a nonuniform magnetic texture can be quantified in units of magnetic field in Tesla as follows:

$$\Delta H_{ex} = \frac{h_{ex} k_B}{\mu_e}. \quad (8)$$

We find that ΔH_{ex} can be as high as 1.3 T for Nb (7 nm)/GdN (3 nm) and reduces to 30 mT for Nb (20 nm)/GdN (3 nm) with increasing niobium film thickness. In Fig. 4, we plot this tunability of the exchange field with niobium film thickness.

We further investigate the in-plane critical field behavior of Nb (7 nm)/GdN, Nb (8 nm)/GdN, and Nb (7 nm)/AlN/GdN films (filled violet and purple circles, and unfilled blue circles, respectively, in Fig. 3) deep inside their respective superconducting states, and track the transition boundary. For Nb/GdN samples we use

$$\frac{h}{T_{c0}} = \frac{\mu_e \mu_0 H_{app}}{K_B T_{c0}} + \frac{h_C}{T_{c0}}, \quad (9)$$

where $\mu_0 H_{app}$ is the magnitude of externally applied magnetic field in Tesla and we assume $h_C = 0$ for Nb/AlN/GdN due to the absence of the proximity effect of GdN on niobium. The critical field of Nb (7 nm)/AlN (3 nm)/GdN (3 nm) is in the order of 11.3 T, and it is comparable to the h_C experienced by Nb (7 nm)/GdN (3 nm). A second-order

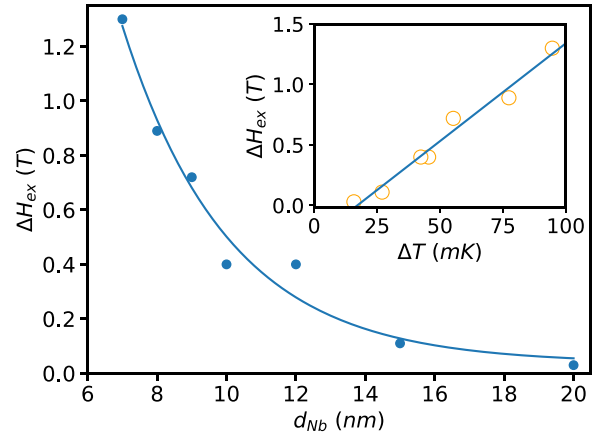


FIG. 4. Degree of tunability (ΔH_{ex}) of the exchange field with varying niobium film thicknesses in Nb/GdN bilayers. Inset: Yellow circles show ΔH_{ex} versus ΔT .

broad transition is evident (refer to Supplemental Material Fig. S2 [24]) at all temperatures for all samples, and yet we observe a deviation from the M-F second-order phase boundary (blue dotted line in Fig. 3). Such deviations are expected for superconductors with appreciable spin-orbit scattering (which includes niobium [32]) as predicted by the Werthamer-Helfand-Hohenberg (WHH) theory [33]. Moreover, per the WHH theory, spin paramagnetic scattering and mean free path are inversely related, and this translates to a higher critical field phase boundary for a higher mean free path. We observe this exact phenomenon when contrasting the data of Nb (7 nm)/GdN (3 nm) (violet circles in Fig. 3) against Nb (8 nm)/GdN (3 nm) (purple circles in Fig. 3). Furthermore, in accordance with WHH predictions, we breach the Chandrasekhar-Clogston limit [34,35] for the Nb (8-nm)/GdN (3-nm) sample at low temperatures.

In conclusion, by controlling the Cooper pair dimensions, both by means of temperature and by changing thickness of the superconductor, our results demonstrate switching on and off of the superconducting state by purely paramagnetic effects of the underlying FI magnetic microstructure. This switching effect is tantamount to large, tunable exchange fields (> 1 T), which is very significant for Majorana zero-mode devices, where local field tunability with minimal external fields are necessary [36–38]. Our results demonstrate that small-area, ultrathin Nb/GdN bilayers are useful candidates for this purpose. Moreover, per our knowledge, this study is the only attempt thus far to compare experimental data with phase diagram of paramagnetically limited DWS. Finally, such paramagnetically limited switchable bilayers can be used for designing cryogenic memory devices with switching fields that are approximately two orders of magnitude lower than that reported for orbitally limited DWS [12].

We thank H. K. Pal, Department of Physics, IIT Bombay, for valuable discussions. We express our sincere thanks to R. J. Choudhary, UGC-DAE CSR, Indore, for helping us carry

out the SQUID VSM measurements. The work was financially supported by a Core Research Grant from the Department of Science and Technology, Science and Engineering Research Board, India (Grant No. CRG/2019/004758).

P.K.S., P.B., and A.P. conceived the experiment. P.B. grew the multilayered samples and performed the low-temperature

magnetotransport measurements. S.B. optimized the thin-film growth recipes for niobium and GdN. B.D. performed SQUID VSM measurements. P.K.S. fabricated Hall bars on the multilayers for residual resistivity measurements. P.B. and A.P. analyzed the data and wrote the manuscript. All authors discussed the results and commented on the manuscript.

-
- [1] J. Linder and J. W. A. Robinson, Superconducting spintronics, *Nat. Phys.* **11**, 307 (2015).
- [2] L. N. Bulaevskii, A. I. Buzdin, and S. V. Panjukov, The oscillation dependence of the critical current on the exchange field of ferromagnetic metals (F) in Josephson junction S-F-S, *Solid State Commun.* **44** 539 (1982).
- [3] T. Kontos, M. Aprili, J. Lesueur, F. Genêt, B. Stephanidis, and R. Boursier, Josephson junction through a thin ferromagnetic layer: Negative coupling, *Phys. Rev. Lett.* **89**, 137007 (2002).
- [4] V. V. Ryazanov, V. A. Oboznov, A. Y. Rusanov, A. V. Veretennikov, A. A. Golubov, and J. Aarts, Coupling of two superconductors through a ferromagnet: Evidence for a Π junction, *Phys. Rev. Lett.* **86**, 2427 (2001).
- [5] F. S. Bergeret, A. F. Volkov, and K. B. Efetov, Long-range Proximity Effects in Superconductor-Ferromagnet Structures, *Phys. Rev. Lett.* **86**, 4096 (2001).
- [6] F. S. Bergeret, A. F. Volkov, and K. B. Efetov, Odd triplet superconductivity and related phenomena in superconductor-ferromagnet structures, *Rev. Mod. Phys.* **77**, 1321 (2005).
- [7] J. W. A. Robinson, J. D. S. Witt, and M. G. Blamire, Controlled injection of spin-triplet supercurrents into a strong ferromagnet, *Science* **329**, 59 (2010).
- [8] T. S. Khaire, M. A. Khasawneh, W. P. Pratt, and N. O. Birge, Observation of spin-triplet superconductivity in Co-based Josephson junctions, *Phys. Rev. Lett.* **104**, 137002 (2010).
- [9] T. Champel and M. Eschrig, Switching superconductivity in superconductor/ferromagnet bilayers by multiple-domain structures, *Phys. Rev. B* **71**, 220506(R) (2005).
- [10] M. Houzet and A. I. Buzdin, Theory of domain-wall superconductivity in superconductor/ferromagnet bilayers, *Phys. Rev. B* **74**, 214507 (2006).
- [11] A. Y. Aladyshkin, A. I. Buzdin, A. A. Fraerman, A. S. Mel'nikov, D. A. Ryzhov, and A. V. Sokolov, Domain-wall superconductivity in hybrid superconductor-ferromagnet structures, *Phys. Rev. B* **68**, 184508 (2003).
- [12] Z. Yang, M. Lange, A. Volodin, R. Szymczak, and V. V. Moshchalkov, Domain-wall superconductivity in superconductor-ferromagnet hybrids, *Nat. Mater.* **3**, 793 (2004).
- [13] L. Y. Zhu, T. Y. Chen, and C. L. Chien, Altering the superconductor transition temperature by domain-wall arrangements in hybrid ferromagnet-superconductor structures, *Phys. Rev. Lett.* **101**, 017004 (2008).
- [14] A. Y. Rusanov, M. Hesselberth, J. Aarts, and A. I. Buzdin, Enhancement of the superconducting transition temperature in Nb/permalloy bilayers by controlling the domain state of the ferromagnet, *Phys. Rev. Lett.* **93**, 057002 (2004).
- [15] B. Li, N. Roschewsky, B. A. Assaf, M. Eich, M. Epstein-Martin, D. Heiman, M. Müntenberg, and J. S. Moodera, Superconducting spin switch with infinite magnetoresistance induced by an internal exchange field, *Phys. Rev. Lett.* **110**, 097001 (2013).
- [16] S. Komori, A. Di Bernardo, A. I. Buzdin, M. G. Blamire, and J. W. A. Robinson, Magnetic exchange fields and domain wall superconductivity at an all-oxide superconductor-ferromagnet insulator interface, *Phys. Rev. Lett.* **121**, 077003 (2018).
- [17] T. Tokuyasu, J. A. Sauls, and D. Rainer, Proximity effect of a ferromagnetic insulator in contact with a superconductor, *Phys. Rev. B* **38**, 8823 (1988).
- [18] F. Aikebaier, P. Virtanen, and T. Heikkilä, Superconductivity near a magnetic domain wall, *Phys. Rev. B* **99**, 104504 (2019).
- [19] X. Hao, J. S. Moodera, and R. Meservey, Thin-film superconductor in an exchange field, *Phys. Rev. Lett.* **67**, 1342 (1991).
- [20] A. Hijano, S. Ilić, M. Rouco, C. González-Orellana, M. Ilyn, C. Rogero, P. Virtanen, T. T. Heikkilä, S. Khorshidian, M. Spies, N. Ligato, F. Giazotto, E. Strambini, and F. S. Bergeret, Coexistence of superconductivity and spin-splitting fields in superconductor/ferromagnetic insulator bilayers of arbitrary thickness, *Phys. Rev. Res.* **3**, 023131 (2021).
- [21] F. S. Bergeret, M. Silaev, P. Virtanen, and T. T. Heikkilä, Colloquium: Nonequilibrium effects in superconductors with a spin-splitting field, *Rev. Mod. Phys.* **90**, 041001 (2018).
- [22] L. R. Tagirov, Low-field superconducting spin switch based on a superconductor/ferromagnet multilayer, *Phys. Rev. Lett.* **83**, 2058 (1999).
- [23] N. Pinto, S. J. Rezvani, A. Perali, L. Flammia, M. V. Milošević, M. Fretto, C. Cassiago, and N. De Leo, Dimensional crossover and incipient quantum size effects in superconducting niobium nanofilms, *Sci. Rep.* **8**, 4710 (2018).
- [24] See Supplemental Material at <http://link.aps.org/supplemental/10.1103/PhysRevB.108.L140502> for R-T versus H color plots of Nb (7, 8, 20 nm)/GdN (3 nm), in-plane R-H data for bilayer Nb (7, 8 nm)/GdN (3 nm) in the range 1.73 to 4.02 K, and for bare Nb (7 nm) at 3.5, 4, and 5 K used for generating Fig. 3. The saturation moment versus temperature profile of 3-nm GdN is also provided.
- [25] A. F. Mayadas, R. B. Laibowitz, and J. J. Cuomo, Electrical characteristics of rf-sputtered single-crystal niobium films, *J. Appl. Phys.* **43**, 1287 (1972).
- [26] A. I. Gubin, K. S. Il'in, S. A. Vitusevich, M. Siegel, and N. Klein, Dependence of magnetic penetration depth on the thickness of superconducting Nb thin films, *Phys. Rev. B* **72**, 064503 (2005).
- [27] F. Natali, B. J. Ruck, N. O. V. Plank, H. J. Trodahl, S. Granville, C. Meyer, and W. R. L. Lambrecht, Rare-earth mononitrides, *Prog. Mater. Sci.* **58**, 1316 (2013).

- [28] R. Vidyasagar, T. Kita, T. Sakurai, T. Shimokawa, and H. Ohta, Ferromagnetic resonance features of degenerate GdN semiconductor, *Phys. Lett. A* **381**, 1905 (2017).
- [29] K. Maki, The behavior of superconducting thin films in the presence of magnetic fields and currents, *Prog. Theor. Phys.* **31**, 731 (1964).
- [30] P. Fulde, High field superconductivity in thin films, *Adv. Phys.* **22**, 667 (1973).
- [31] K. Maki, Pauli paramagnetism and superconducting state. II, *Prog. Theor. Phys.* **32**, 29 (1964).
- [32] I. Zaytseva, A. Abaloszew, B. C. Camargo, Y. Syryanyy, and M. Z. Cieplak, Upper critical field and superconductor-metal transition in ultrathin niobium films, *Sci. Rep.* **10**, 19062 (2020).
- [33] N. R. Werthamer, E. Helfand, and P. C. Hohenberg, Temperature and purity dependence of the superconducting critical field, H_{c2} : III. Electron spin and spin-orbit effects, *Phys. Rev.* **147**, 295 (1966).
- [34] B. S. Chandrasekhar, A note on the maximum critical field of high-field superconductors, *Appl. Phys. Lett.* **1**, 7 (1962).
- [35] A. M. Clogston, Upper Limit for the critical field in hard superconductors, *Phys. Rev. Lett.* **9**, 266 (1962).
- [36] L. Fu and C. L. Kane, Superconducting proximity effect and Majorana fermions at the surface of a topological insulator, *Phys. Rev. Lett.* **100**, 096407 (2008).
- [37] J. D. Sau, R. M. Lutchyn, S. Tewari, and S. D. Sarma, Generic new platform for topological quantum computation using semiconductor heterostructures, *Phys. Rev. Lett.* **104**, 040502 (2010).
- [38] S. Vaitiekėnas, Y. Liu, P. Krogstrup, and C. M. Marcus, Zero-bias peaks at zero magnetic field in ferromagnetic hybrid nanowires, *Nat. Phys.* **17**, 43 (2021).